Correlation between thermal properties and aluminum fractions in CrAlN layers deposited by PVD technique

B. Tlili [a,b,*], N. Mustapha [a,1], C. Nouveau [b,2], Y. Benlatreche [b,2], G. Guillemot [c,3], M. Lambertin [b,2]

[a] UR. Mécanique Appliquée, Ingénierie et Industrialisation (M.A2I), ENIT, BP 37 Le belvédère 1002 Tunis, Tunisie
[b] Laboratoire Bourguignon des Matériaux et Procédés (LABOMAP), CER ENSAM de Cluny, Rue Porte de Paris, F-71250 Cluny, France
[c] Laboratoire de Métallurgie Physique et Génie des Matériaux, Equipe Caractérisation et Propriétés de la Périsurface, CNRS UMR 8517, Ecole Nationale Supérieure d'Arts et Métiers, 8 Boulevard Louis XIV 59046 Lille cedex, France

Keywords:
Density
Residual stress
Conductivity
CrAlN
Microstructure

A B S T R A C T

The CrAlN coatings are a good alternative to conventional CrN coatings especially for high temperature oxidation-resistance applications. Different CrAlN coatings were deposited on silicon (100) by PVD (Physical vapor deposition) technique from two targets (chromium and aluminum) in a reactive nitrogen atmosphere at aluminum applied negative voltage (−300, −500, −700 and −900 V). The composition, structural, mechanical and thermal properties of the as-deposited coatings were systematically characterized by energy dispersive analysis of X-rays, X-ray diffraction, nanoindentation, and the "Mirage effect" experiments.

The X-ray diffraction (XRD) data show that in general CrAlN coatings were crystallized in the cubic NaCl B1 structure, with the (1 1 1) and (2 0 0) diffraction peaks observed. Two-dimensional surface morphologies of CrAlN coatings were investigated by atomic force microscope (AFM). The results show that with increasing aluminum proportion the coatings became more compact and denser and their increased correspondingly, showing a maximum hardness of about 36 GPa (30 at% of Al) which is higher than that of CrN. Moreover, the results in this work demonstrate that the variation of aluminum fraction alter the resulting columnar grain morphology and porosity of the coatings. However, the thermal properties are greatly affected by these morphological alterations. The correlation between aluminum fraction in CrAlN coatings and its thermal properties revealed that the conductivity and the diffusivity are influenced primarily by size and shape distribution of the pores and secondarily by a decrease of the stitch parameter dimension.

1. Introduction

As a kind of hotworking mechanical pieces, AISI4140 steel undergoes wear caused by mechanical contact action under a high pressure, corrosive attack, thermal cycling, high temperature corrosion (oxidation), and very large surface loads. The use of PVD hard coatings such as TiN, CrN and TiAlN, in order to improve the lifetime of mechanical parts is a well-known approach. Hard coatings can protect the steel surface very efficiently from physico-chemical attacks and delay the formation and propagation of thermal and mechanical cracks [1]. In recent years, chromium aluminum nitride (CrAlN), a ternary nitride obtained by incorporating Al into transition binary CrN thin coatings, has been intensively investigated [2–11]. CrAlN coatings have been reported to exhibit good oxidation-resistance with no compositional and structural changes after annealing at 800 °C [5] and at 900 °C [8], as both the chromium and aluminum could form protective oxides which suppressed diffusion of oxygen in the bulk. In addition, CrAlN also exhibits thermal conductivity lowers than that of CrN, good tribological properties and high hardness [6,7]. Therefore, CrAlN coating is a good candidate as an alternative to conventional

CrN coatings, especially for high temperature oxidation-resistance applications.

In this work, thin CrAlN layers were deposited onto silicon (100) substrate using an unbalanced magnetron sputtering technique. The effect of aluminum content on morphology and structure was investigated. The thermal and mechanical properties of the as-deposited coatings were determined. The failure mechanism and the relationships between the thermal properties, such as diffusivity and conductivity, and the density behavior were discussed.

2. Experimental

A thin film layer of CrAlN is deposited onto samples of silicon, with different aluminum (Al) atomic percent. The film deposition was carried out by a dual RF magnetron sputtering system (NORDIKO type 3500–13.56 MHz) from two targets of high purity (99.999% at Cr, 99.999% at Al) with 10 cm of diameters. Prior to deposition, the samples were polished and then cleaned with acetone in an ultrasonic container for 15 min. Subsequently, they were rinsed in deionized water, dried and stored in desiccators prior to coating deposition. The targets were sputter cleaned for 5 min. Then the samples were sputter-etched with argon ions (10 mbar, applied bias voltage −500 V) for approximately 10 min to remove surface oxide and pollution. All of the two targets were sputtered using RF (Radio Frequency) power. During deposition, the substrate temperature was 150 °C. The sputtering power applied onto Al targets and Cr targets was varied between 3.6 kW and 2.4 kW, respectively. Table 1 lists the principal deposition parameters of the CrAlN coatings. Very high purity Nitrogen was introduced into the vacuum chamber. The pressure in the deposition chamber was 10^{-6} mbar. The distance between the target and surface backing was 10 cm. Moreover, the samples were mounted on a continuously rotating planetary holder inside the vacuum chamber. The atmosphere was chosen in order to produce a CrAlN layers.

The composition of the as-deposited coatings was measured by energy dispersive analysis of X-rays (EDX), which is attached to a scanning electron microscope, at 10 keV and the INCA quantitative analysis software. Alumina and chromium were used as the reference materials for quantitative analyses. The coating structure and residual stresses were analyzed by X-ray diffraction (XRD) which was performed on a Philips X-ray diffractometer in a θ–2θ scanning mode using CuK_α radiation (40 kV, 30 mA). The scanning step size and the counting time at each step were set as 0.05° and 10 s, respectively. micro-hardness of the coatings was measured using a Nanotest 550 nanoindenter equipped with a Berkovich diamond indenter (a three-sided pyramid) .The maximum indentation depth was set at 150 nm, which is less than one tenth of the coating thickness, and therefore the substrate effect on the measured micro-hardness can be neglected [12]. The micro-hardness measurements were calibrated using a fused silica standard sample with hardness around 8.8 GPa, and the maximum indentation depth for calibration was also set at 150 nm. For each sample, eight points were measured and the average micro-hardness and standard deviation were

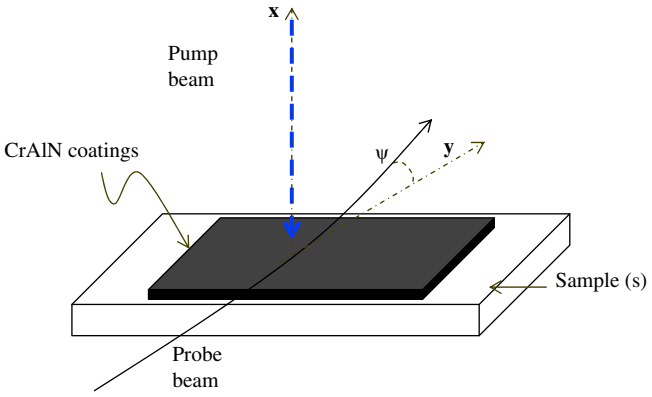

Fig. 1. Schematic representation of the probe beam deflection.

obtained. The residual stress was determined using the Newton method. This method is based on the principle expressed by Stoney [13]. The coating surface morphology and surface roughness were examined by atomic force microscope (AFM).

Finally, the thermal properties are determined by the "Mirage effect" [14,15]. This method consists of heating a sample with a modulated light beam of intensity $I = I_0\ (1 + \cos\ (\omega t))$, $\omega = 2\pi f$, where f is the modulation frequency (Fig. 1) [16]. The warmth absorbed diffuses in the surrounding fluid producing a refractive index gradient. A probe laser beam skimming the surface sample which passes into the refractive index gradient zone undergoes a deflection noted as ψ. This deflection is related to the surface temperature and to the thermal properties of the sample and the various neighboring media.

The CrAlN coating is deposited on a (100) silicon (Si). Before the determination of his thermal properties, the probe beam deflection is deduced using the heat equation in all media and using the beam radius equation in inhomogeneous refractive index medium. We then obtain the following expression:

$$\psi = |\psi| e^{j(\omega t+\varphi)} = \frac{\sqrt{2}l}{n\mu_f}\frac{dn}{dT_f}|T_0| e^{-\frac{x}{\mu_f}} e^{j\left(\theta+\frac{5\pi}{4}-\frac{x}{\mu_f}\right)} e^{j\omega t} \quad (1)$$

Where T_0 is the temperature on the sample surface.

$$\begin{aligned} T_0 = E\Big[&(1-b)e^{-\sigma_s l_s}\Big[(1-r)(1-c)e^{\sigma_c l_c} + (1+r)(1+c)e^{-\sigma_c l_c} \\ &- 2(1+rc)e^{-\alpha l_c}\Big] - (1+b)e^{\sigma_s l_s}\Big[(1-r)(1+c)e^{\sigma_c l_c} \\ &+ (1+r)(1-c)e^{-\sigma_c l_c} - 2(1-rc)e^{-\alpha l_c}\Big]\Big] \Big/ \Big[(1+b)e^{\sigma_s l_s} \\ &\times\Big[(1+g)(1+c)e^{\sigma_c l_c} + (1-g)(1-c)e^{-\sigma_c l_c}\Big] \\ &-(1-b)e^{-\sigma_s l_s}\Big[(1+g)(1-c)e^{\sigma_c l_c} + (1-g)(1+c)e^{-\sigma_c l_c}\Big]\Big] \end{aligned} \quad (2)$$

Table 1
Deposition conditions.

Coating	Working pressure (μbar)	Applied voltage (V)		Rotation velocity (rpm)	Time (min)	Temperature (°C)	Gas pressure (mbar)	
		Al	Cr				Ar (80%)	N_2 (20%)
CrAlN	4	0 −300 −500p −700 −900	−900	0.5	90	150	4.10^{-3}	4.10^{-3}

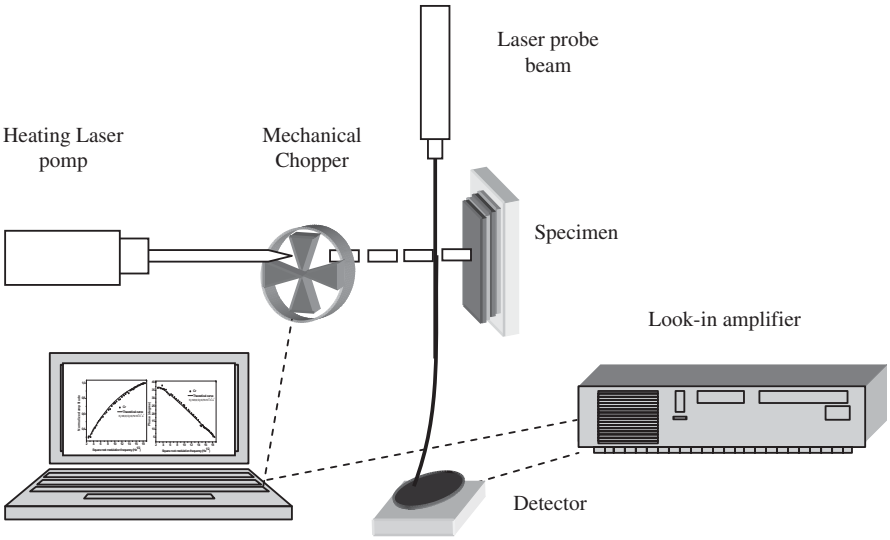

Fig. 2. Schematic experimental set-up.

with

$$b = \frac{K_b}{K_s}\sqrt{\frac{D_s}{D_b}}, c = \frac{K_c}{K_s}\sqrt{\frac{D_s}{D_c}}, g = \frac{K_f}{K_c}\sqrt{\frac{D_c}{D_f}}, r = \frac{(1-j)\alpha}{2\mu_c}, \sigma_i = (1+j)\sqrt{\frac{\pi f}{D_i}}$$

Where K_i, D_i, and μ_i are respectively the thermal conductivity, the thermal diffusivity and the thermal length of the (i) medium (f, c, s, b) designating the fluid as 'f', the black graphite layer as 'c', the substrate as 's' and the backing a 'b'.

$$|\psi| = \frac{\sqrt{2}l}{n\mu_f}\frac{dn}{dT_f}|T_0|e^{-\frac{x}{\mu_f}} \tag{3a}$$

and

$$\varphi = -\frac{x}{\mu_f} + \theta + \frac{5\pi}{4} \tag{3b}$$

$|\Psi|$ and φ amplitude and phase of the probe beam deflection. $|T_0|$ and θ are respectively the amplitude and phase of the sample's surface temperature.

The experimental set-up shown on (Fig. 2) is described in detail in ref [14–16]; it is composed of a halogen heating lamp, a laser probe beam, a photo-detector position sensor and a look-in amplifier. The light coming from the halogen lamp is modulated by a mechanical chopper. A laser prop beam skimming the sample surface is deflected. Its deflection is measured by a position photo-detector sensor.

3. Results and discussion

3.1. Mechanical properties of deposited layers

Table 2 summarizes the different properties of the synthesized CrAlN coatings. The Al content in CrAlN films varies between 0 and 30%. We can note that in the CrAlN deposited films, the hardness varies between 16 and 36 GPa which exceeds the hardness of the conventional Cr–N system, which is approximately of 9.3 GPa [17,18]. Besides, a high Young modulus (which varies between 400 and 460 GPa) has been measured compared a bulk CrN (256 ± 8 GPa) [18], the same results were obtained by Kim and Lee [19].

The relationship between the residual stress and the aluminum applied voltage was synthesized; the mean of the compressive residual stress value is about −2 MPa. It can be seen that all the samples exhibit contract stress and the value of residual stress increases with the increasing of aluminum applied voltage. The sample deposited at −900 V has the highest compressive residual stress with a value of −3.6 MPa. The CrAlN thin films were deposited at the same temperature, so the thermal stresses of all the thin films were presumed to be the same.

Differences of the residual stresses may be ascribed to the variations of intrinsic and extrinsic stresses [20]. Various models have been invoked to explain the origin of intrinsic stress [21,22]. From these literature data, the magnitude of intrinsic stresses in PVD films is found to be related to their microstructure, i.e., morphology, texture, grain size depicted by the structure-zone diagrams. The grain boundary relaxation (GBR) model proposed by Hoffman [22] can account for the increase of residual stresses, which is due to crystallite sizes decrease. However, low residual stresses (between −1 and −3.6 GPa) as obtained by Reiter et al. [23] were determined, which promotes good adhesion of the CrAlN layers. In addition, these low residual stresses will enable us to deposit thick films (between 1.8 and 3 μm), which reduces cracks produced by alternating and thermal stresses, and leads to good mechanical and tribological properties [6].

3.2. Micro-structural and morphological characterization

The mean Al to Cr atomic ratio determined by the EDX analyses in the as-deposited CrAlN coatings as a function of the applied

Table 2
Properties of CrAlN deposited films.

Aluminum applied voltage (V)	Thickness (μm)	Al content (at. %)	Atomic ratio of Al/Cr	Surface roughness Rms (nm)	Hardness (GPa)	Young's modulus (GPa)	Residual stress (GPa)
0	1.8	0	0	9	24	400	1
−300	2.1	5	0.08	9.8	26	410	1.1
−500	2.5	13	0.26	16.5	26	410	1.5
−700	2.7	28	0.64	21.3	23	380	1.4
−900	3	30	0.7	25.1	36	460	3.6

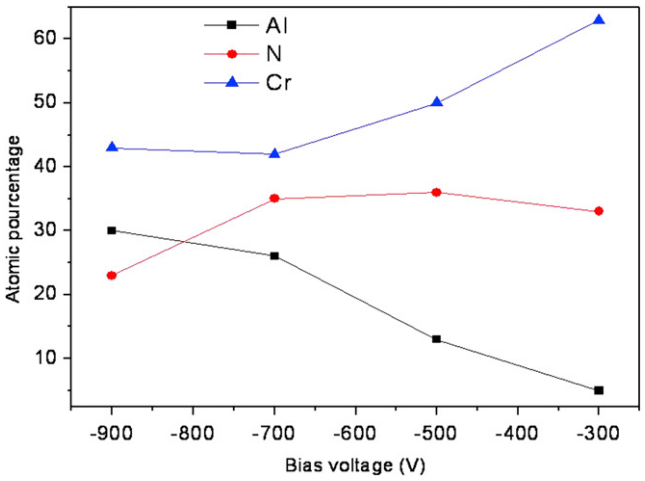

Fig. 3. Atomic percentage evolution with aluminum applied voltage, −900 V, −700 V, −500 V, −300 V and 0 V (the thickness of the coating layers is correspondingly: 3 μm, 2.7 μm, 2.5 μm, 2.1 μm and 1.8 μm).

voltage onto the aluminum target. It is as expected that the Al/Cr atomic ratio in the coatings increased monotonically with the increase of the aluminum applied voltage. It was noted that for each coating sample, the Al/Cr atomic ratio is much lower than the current ratio. This fact could be ascribed to the formation of an insulating AlN layer on Al cathode surface during coating deposition. The maximum Al/Cr atomic ratio in the as-deposited coatings is about 0.7, beyond which no complete coatings could be deposited. The measured nitrogen content in all of the as-deposited CrAlN coatings was about 35%, as shown in Fig. 3.

Fig. 4 shows the morphology of CrAlN layers determined by aluminum applied voltage −500 V and −900 V respectively. In general, the layer growth begins with the arrival of the aluminum and chromium atoms, where it will have formation of matter into small islands by nucleation and growth. Hones [24] schematized this process of deposit as the growth of columns that take on the shape of cones of various diameters. For the first atomic layers (low thicknesses of the deposit), we are in presence of closer columns relatively identical and stuck, who causes its progressive thickening. This observation by SEM on a cross-section shows that the columns are perpendicular to the backing surface (Fig. 4 A). In contrast the coating with highest aluminum applied voltage (Fig. 4 B) shows a finer and denser isotropic structure. The change in coating structure can be explained by considering Thornton's deposition model [25]. The assumption is that due to the reactive heat, atom mobility is increased; leading to a denser isotropic structure.

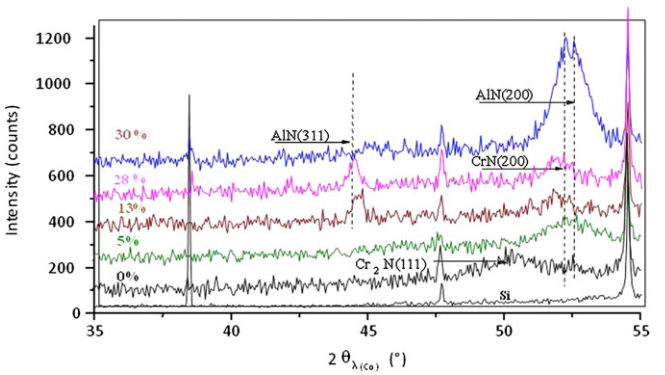

Fig. 5. XRD diffractogram of the as-deposited CrAlN coatings with different aluminum proportion onto silicon (the thickness of the coating layers is correspondingly: 3 μm, 2.7 μm, 2.5 μm and 2.1 μm).

Fig. 5 shows the XRD diffractogram of the as-deposited CrAlN coatings. All coatings were well crystallized. Besides the XRD peaks arisen from the Si substrate (marked as Si in the figure), other two evident peaks at around $2\theta = 37.5°$ and 43.6° could be attributed to the rocksalt-type cubic phase CrN (111) and (200), respectively, similar to Ref. [26,27]. Generally, the intensity of all these two diffraction peaks increased, implying an increase in coating crystallinity, gradually with increasing aluminum fraction. This fact could be attributed to the lattice distortion caused by aluminum incorporation. The dependence of CrN (111) peak position on the aluminum fraction can be noted. Another side, it is important to note the appearance of peak (111) of CrN, well-defined net at 13% of Al and net at least 28%. The EDS analysis of these films shows that these CrAlN points report N/Cr is lowest, then it is estimated that these films consist of nanocrystals of CrN/AlN, which also reflected in the morphology by a dense structure.

The CrN (111) peak shifted to the higher angle side, indicating a gradual decrease of lattice parameters with increasing aluminum fraction except for the very weak peak at 30% of Al. This phenomenon indicates the formation of the pseudo binary alloy CrAlN and the lattice shrinking fact could be ascribed to the replacement of chromium atoms by the smaller aluminum atoms. On one hand, this fact could be interpreted as the substitution of Cr atoms with the smaller Al ones, which results in the contraction of the CrN lattice. On the other hand, from Ref. [26], it is noted that the position of this peak coincides well with the hexagonal aluminum nitride h-AlN (004) reflection when the Al/Cr atomic ratio is greater or equal to 1.6, therefore this peak's shift to a higher angle side could also be partially related to phase separation of h-AlN from the supersaturated solid solution of CrAlN. Although the maximum

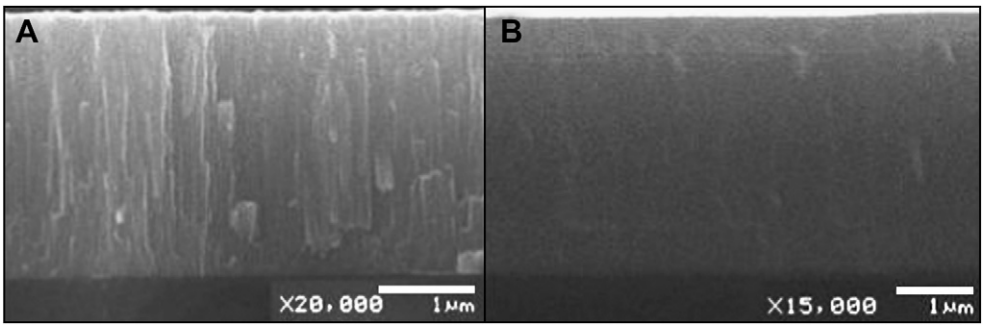

Fig. 4. Scanning electron micrograph (SEM) of a cross-section of CrAlN coatings as made by fractography, at −500 (A) and −900 V (B) (the thickness of the coating layers is correspondingly: 2.5 μm and 3 μm).

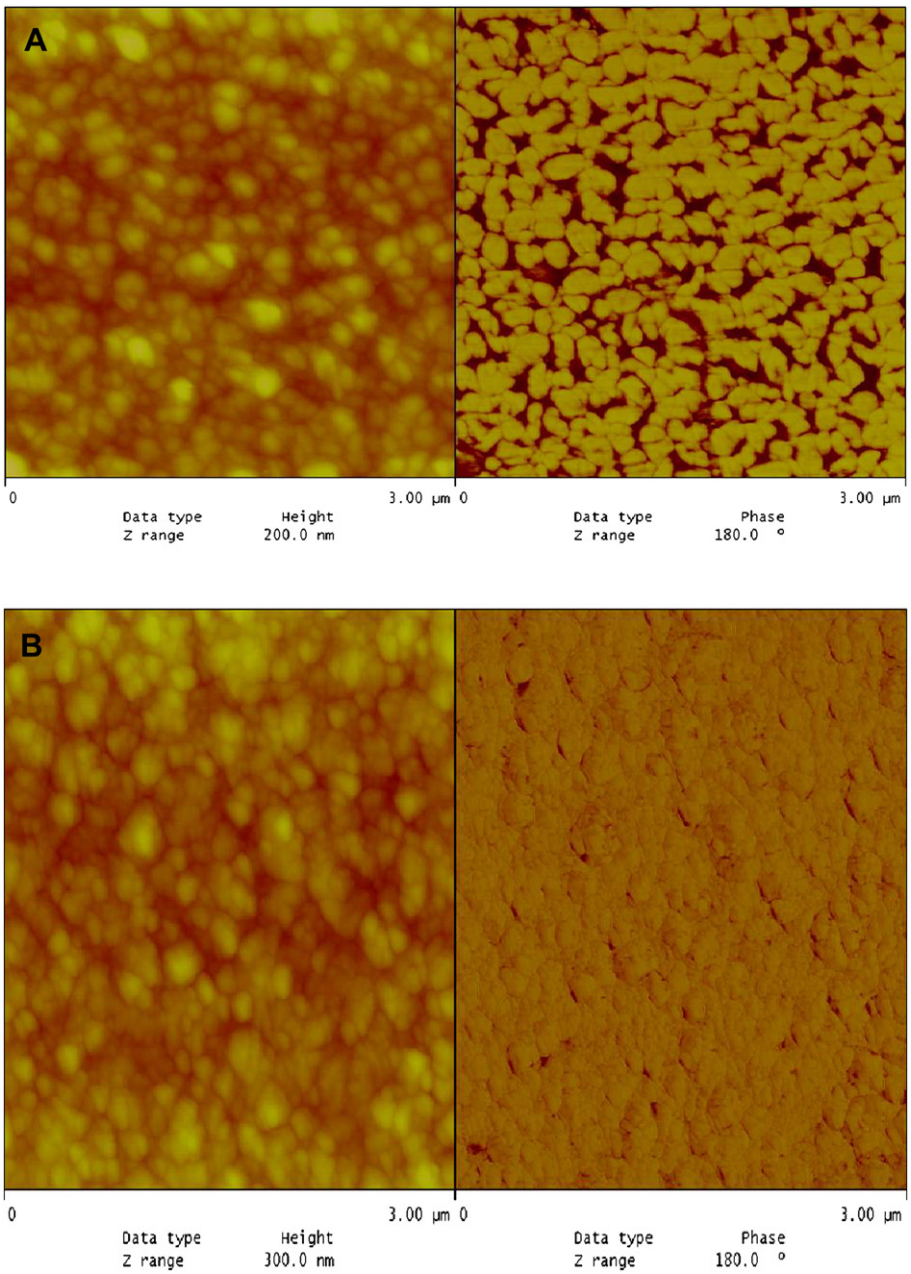

Fig. 6. Two-dimensional AFM surface morphologies of CrAlN coatings deposited under different aluminum applied voltage: (A) −300 V and (B) −500 V (the thickness of the coating layers is correspondingly: 1.8 μm and 2.5 μm)

solubility of AlN in cubic CrN has been predicted to go as high as 77 mol% [28,29]; the supersaturated CrAlN phase is thermodynamically metastable and the actual solubility limit strongly depends on the deposition conditions [30,31]. Moreover, it was found that with the incorporation of Al into the CrN coating, the full width at half maximum (FWHM) of the (111) diffraction peak increased, indicating an decrease of crystal size in the CrAlN coating in comparison with that in the CrN coating, meanwhile the coating hardness was significantly enhanced due to the solid solution hardening effect. As shown in Fig. 5, the diffraction peak position of CrN (200) moves to the right as the aluminum applied voltage increases and the interplanar distance decreases. The decrease of interplanar distance (or increase of 2θ) implies the increase of compressive residual stress. This is because tensile stress parallel to the surface causes vertical contraction of the film in the θ–2θ mode of XRD measurement and leads to a decrease of interplanar distance, which is parallel to the surface. Therefore, the evolution of residual stresses can be explained by above factors responsible for compressive residual stress generation appear to be more and more active with the increase of aluminum applied voltage.

From the analysis of residual stress mentioned above, the reason for increases of compressive stress with the aluminum fraction is the variation of intrinsic stresses and extrinsic stresses. As can be seen in Fig. 5, the preferential orientation change is evident. In our case, all the films are apt to show a (200) texture at high aluminum fractions except (111) texture at lower aluminum fractions (13% of Al). So this evolution is difficult to understand, all the more so as the authors have found that, under some given conditions (substrate

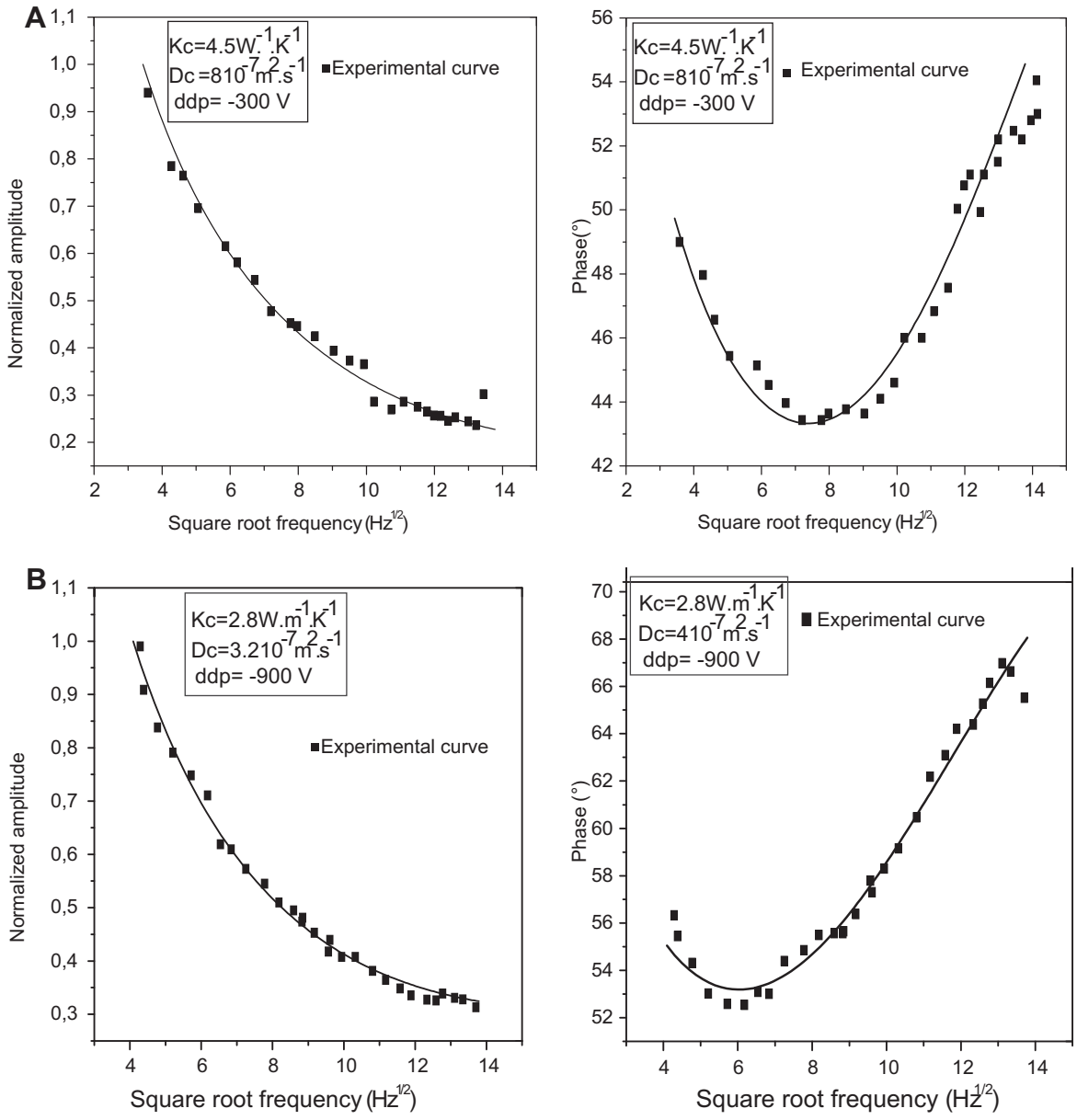

Fig. 7. Normalized amplitude and phase evolution of the photo thermal signal vs the square root frequency of the deposited CrAlN layers obtained at −300 V (A) and −900 V (B) (the thickness of the coating layers is correspondingly: 1.8 μm and 3 μm).

temperature and deposition rate [32], or film thickness [33]), the coatings would present a preferential orientation corresponding to the crystallographic planes which have the highest reticular density. For cubic CrAlN structure, the order of reticular increase is (111) < (200). The texture modification observed when aluminum fraction varies can certainly be attributed to the intrinsic stress evolution in the films. Therefore, this lower compressive stress can explain the development of the texture built on less dense (111) planes including higher number of point defects and the higher stress results from the deposition along (200) orientation with a dense structure. So the evolution of residual stress can be ascribed to the complicated structure variation of CrAlN thin films.

Two-dimensional surface morphologies of CrAlN coatings deposited at different aluminum applied voltage were measured by AFM (Fig. 6). With increasing aluminum applied voltage, the coating became more compact and denser. The overall surface roughness values of CrAlN coatings deposited at different negative substrate bias voltages are summarized in Table 2. Coating surface roughness increased with an increase of aluminum applied voltage. The change in coating surface roughness and morphology can be explained by the ion energy/ion flux change. The increase of aluminum applied voltage results in an increased mobility of the atoms and a higher nucleation density [34]. Consequently denser coatings can be formed, as can be seen in Fig. 6 B. In addition, the highly mobile adatoms can move or diffuse into the inter-grain voids under the high energy ion bombardment and a denser structure is attained [35–37].

3.3. Thermal properties

In order to determine the thermal properties of the CrAlN layers, we plotted into Fig. 7 the experimental variation of phase and

normalized amplitude of the PDT signal versus the square root modulation frequency. The difference between these curves is attributed to the difference of their thermal conductivity and thermal diffusivity. Using the theoretical model presented in ref [14,15], one can deduce both thermal conductivity and thermal diffusivity parameters (K, D). The coincidence between experimental and theoretical curves is obtained for a known and unique value of K and D.

On (Fig. 8) are plotted the thermal conductivity and the thermal diffusivity versus the aluminum applied voltage. The conductivity and thermal diffusivity of CrAlN coatings decrease gradually if the aluminum fraction in the layers is increased (aluminum applied voltage increases in absolute value), and finally moves towards stabilized values 2.8 W $m^{-1} K^{-1}$ for thermal conductivity and 4×10^{-7} $m^2 s^{-1}$ for thermal diffusivity. The thermal properties become constant for a percentage of aluminum higher than 28% (bias < -700 V) which may be explained by a stabilization of the crystalline structure. The same result is already proved in the determination of the morphology and residual stresses [30,31]. Moreover, to investigate the reason for the lower thermal conductivity, the microstructure of the coatings was observed by SEM (Fig. 4). For the coating with addition of 13% (-500 V aluminum applied voltage) of aluminum, the column shows a relatively dense structure although feather-like sub-column pores are also observed. In contrast, a finer distribution of feather-like sub-column pores is found in the coating containing is about 30% (-900 V aluminum applied voltage) of aluminum, which would contribute to a reduction in thermal conductivity [38]. It is known that nanostructures of PVD films are formed by rotating substrates during deposition. The substrate rotation leads to the continuous change in the incidence angle of aluminum vapor, resulting in the formation of columnar grains as well as feather-like pores [39]. However, we interpret the decrease in thermal conductivity with aluminum fraction by the decrease of the phonon mean free path λ. As the phonon may be considered like a quasi-particle which obey the kinetic theory of gases, then the thermal conductivity related to the phonon mean free path λ by through the following expression [14,15].

$$K = \frac{\rho c v}{3}\lambda \tag{4}$$

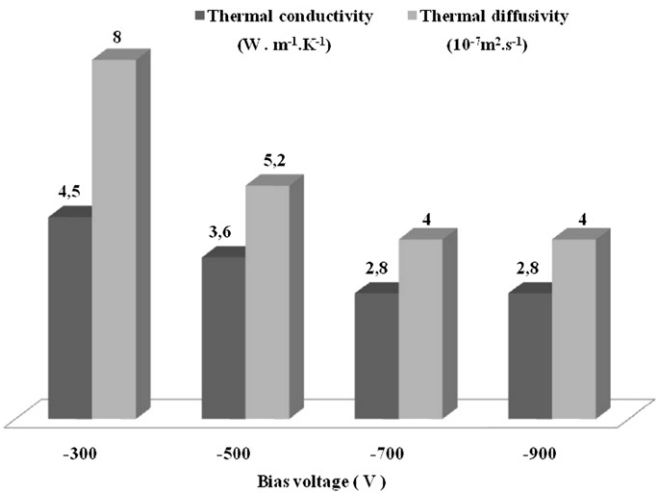

Fig. 8. Thermal properties evolution versus aluminum applied voltage: -900 V, -700 V, -500 V and -300 V (the thickness of the coating layers is correspondingly: 3 μm, 2.7 μm, 2.5 μm and 2.1 μm).

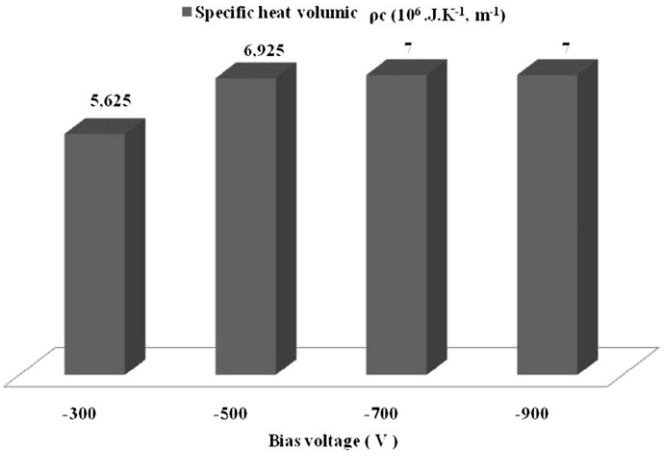

Fig. 9. Volumic specific heat evolution versus aluminum applied voltage: -900 V, -700 V, -500 V and -300 V (the thickness of the coating layers is correspondingly: 3 μm, 2.7 μm, 2.5 μm and 2.1 μm).

where, ν is the mean speed of the particles of a diluted gas at room temperature whose value is : $\nu = 3500$ m s^{-1}.

Moreover, the relationship between the thermal conductivity and the thermal diffusivity give the specific heat volumic (ρ c), which is inversely proportional to the porosity. In this work, the evolution of the latter based on the fraction of aluminum in CrAlN layers. This gives an idea on evaluating desired porous coatings (Fig. 9).

Developments of specific heat volumic (ρc) depends on the aluminum applied voltage is a curve which stabilizes at the extreme conditions (28% up to 30% of aluminum), which indicates low porosity. Hence, when the aluminum fraction increases in CrAlN layers, the porosity will be reduced. This can be explained by the effect of mesh parameters, the amorphous structure, and the role of crystalline defects on the intrinsic properties (plasticity, reactivity, diffusivity …).

4. Conclusion

In the present work, the investigation of micro-structural and mechanical properties of CrAlN coating deposited on silicon substrate and specially the effect of the aluminum proportion on their physical properties were presented

1. The mean Al to Cr atomic ratio increased with increasing aluminum applied voltage. All films crystal phase, and both the crystal orientation and the crystallite size depended on deposition parameters and various aluminum content.
2. All the CrAlN films exhibited compressive stress depends on varying aluminum content. Generally, the value of residual stress increased with increasing of aluminum fraction, this is proven by the value of the compressive residual stresses that can reach up to 3.6 GPa for 30% of aluminum. Therefore, the CrAlN films present many important mechanical properties (the Young modulus and hardness). For an aluminum fraction of 30%, these parameters are respectively 36 GPa and 460 GPa. This improves the layer adhesion to the substrate.
3. The thermal properties of CrAlN coatings decreased gradually with decreasing aluminum percentage until a saturation level of 28% and 30% of aluminum is reached.
4. The specific heat volumic shows that the porosity of the CrAlN layers decreases by increasing the aluminum content and then stabilizes for an aluminum fraction of about 20% of aluminum.

This can be attributed to the reduction in the cell parameters and the crystalline defects present in the CrAlN layers. The specific heat volumic of these coatings is principally influenced by the shape of the pores and secondarily by the pore surface area available at the cross section perpendicular to the heat flux.

5. The analysis of experimental results explains that the evolution of thermal properties and residual stress can be attributed to the variation of microstructure in CrAlN thin films as a function of aluminum fraction and deposition parameters.

Acknowledgements

The authors want to thank especially Mr. A. IOST (Pr. ENSAM, Lille) for his advice and collaboration during this work. We also appreciated the contribution of Y. Benlatreche, PhD student in our laboratory.

References

[1] Navinsêk B, Panjan P, Urankar I, Cvahte P, Gorenjak F. Surf Coat Technol 2001;142–144:1148–54.
[2] Barshilia HC, Deepthi B, Selvakumar N, Rajam AKS. Appl Surf Sci 2007;253:5076–83.
[3] Lin J, Mishra B, Moore JJ, Sproul WD. Surf Coat Technol 2006;201:4329–34.
[4] Scheerer H, Hoche H, Broszeit E, Schramm B, Abele E, Berger C. Surf Coat Technol 2005;200:203–7.
[5] Brizuela M, Garcia-Luis A, Braceras I, Oñate JI, Sãnchez-Lõpez JC, Martînez-Martînez D, et al. Surf Coat Technol 2005;200:192–7.
[6] Benlatreche Y, Nouveau C, Marchal R, Ferreira Martins J-P, Aknouche H. Wear 2009;267:1056–61.
[7] Wang L, Nie X, Housden J, Spain E, Jiang JC, Meletis EI, et al. Surf Coat Technol 2008;203:816–21.
[8] Kawate M, Hashimoto AK, Suzuki T. Surf Coat Technol 2003;165:163–7.
[9] Ding X-Z, Zeng XT. Surf Coat Technol 2005;200:1372–6.
[10] Gannon PE, Tripp CT, Knospe AK, Ramana CV, Deibert M, Smith RJ, et al. Surf Coat Technol 2004;188–189:55–61.
[11] Uchida M, Nihira N, Mitsuo A, Toyoda K, Kubota K, Aizawa T. Surf Coat Technol 2004;177–178:627–30.
[12] Oliver WC, Pharr GM. J Mater Res 1992;7:1564.
[13] Wang Q, Ishikawa H, Nakano S, Ogiso H, Akedo J. Vacuum 2004;75:225–9.
[14] Ghrib Taher, Bejaoui Fatah, Hamdi Abdelwahheb, Yacoubi Noureddine. Thermochimica Acta 2008;473:86–91.
[15] Ghrib Taher, Yacoubi Noureddine, Saadallah Faycel. Sens Actuators 2007;A135:346–54.
[16] Ghrib Taher, Salem Sahbi Ben, Noureddine Yacoubi. Tribol Int 2009;42: 391–6.
[17] Barshilia CH, Selvakumar N, Deepthi B, Rajam KS. Surf Coat Technol 2006;201:2193–201.
[18] Okumiya M, Griepentrog M. Surf Coat Technol 1999;112:123–8.
[19] Kim GS, Lee SY. Surf Coat Technol 2006;201:4361–6.
[20] Pauleau Y. Vacuum 2001;61:175.
[21] Grovenor CRM, Hentzell HTG, Smith DA. Acta Metall 1984;32:773.
[22] Hoffman RW. Thin Solid Films 1976;34:185.
[23] Reiter AE, Derflinger VH, Hanselmann B, Bachmann T, Sartory B. Surf Coat Technol 2005;200:2114–22.
[24] Phones. Thèse de doctorat n ◦ 2116. école polytechnique fédérale de Lausanne; 2000. pp. 301–315.
[25] Thornton JA. J Vac Sci Technol 1974;11:666.
[26] Ding Xing-zhao, Zeng XT, Liu YC, Fang FZ, Lim GC. Thin Solid Films 2008;516:1710–5.
[27] Willmann H, Mayrhofer PH, ÂPersson PO, Reiter AE, Hultman L, Mitterer C. Scr Mater 1847;2006:54.
[28] Sugishima A, Kajioka H, Makino Y. Surf Coat Technol 1997;97:590.
[29] Makino Y, Nogi K. Surf Coat Technol 1998;98:1008.
[30] PalDey S, Deevi SC. Mater Sci Eng A Struct Mater Prop Microstruct Process 2002;342:58.
[31] Mayrhofer PH, Mitterer C, Hultman L, Clemens H. Prog Mater Sci 2006;51:1032.
[32] Grantscharova E. Thin Solid Films 1993;224:28.
[33] knuyt G, Quaeyhaegens C, 'Haen JD, Stals LM. Thin Solid Films 1995;258:159.
[34] Cunha L, Andritschky M, Pischow K, Wang Z. Thin Solid Films 1999;355–356: 465–71.
[35] Lin Jianliang, Moore John J, Mishra Brajendra, Pinkas Malki, Sproul WD, Rees JA. Surf Coat Technol 2008;202:1418–36.
[36] Ben Cheikh Larbi A, Tlili B. Surf Coat Technol 2006;201:1511–8.
[37] Tlili B, Nasri M, Ayari F, Nouveau C. International Review of Mechanical and Engineering; 2008. 2 Mars; V2.
[38] Lu TJ, Levi CG, Wadley HNG, Evans AG. J Am Ceram Soc 2001;84:2937.
[39] Terry SG, Litty JR, Levi CG. Metals and Materials Society 1999;13.